https://ieeexplore.ieee.org/document/8868230

DOI: 10.1109/TITS.2019.2946324

Nonlinear Moving Horizon Estimation for Large-scale Urban Road Networks

Isik Ilber Sirmatel and Nikolas Geroliminis

***Abstract*—Perimeter control schemes proposed to alleviate congestion in large-scale urban networks usually assume perfect knowledge of the accumulation state together with current and future inflow demands, requiring information about the origins and destinations (OD) of drivers. Such assumptions are problematic for practice due to: (i) Measurement noise, (ii) difficulty of measuring OD-based accumulation states and inflow demands. To address these, we propose a nonlinear moving horizon estimation (MHE) scheme for large-scale urban road networks with dynamics described via macroscopic fundamental diagram. Furthermore, we consider various measurement configurations likely to be encountered in practice, such as measurements on regional accumulations and transfer flows without OD information, and provide results of their observability tests. Simulation studies, considering joint operation of the MHE with a model predictive perimeter control scheme, indicate substantial potential towards practical implementation of MFD-based perimeter control.**

***Index Terms*—Moving horizon estimation (MHE), traffic state estimation, model predictive control (MPC), macroscopic fundamental diagram (MFD), large-scale urban road networks.**

I. Introduction

MODELING, estimation, and control of large-scale urban road networks present considerable challenges. Inadequate infrastructure and coordination, low sensor coverage, spatiotemporal propagation of congestion, and the uncertainty in traveler choices contribute to the difficulties faced when creating realistic models and designing effective estimation and control schemes for urban networks. Although considerable research has focused on real-time traffic control in the last decades, estimation and control of heterogeneously congested large-scale networks remains a challenging problem.

Studies on traffic modeling and control for urban networks usually focus on microscopic models keeping track of link-level traffic dynamics with control strategies using local information. Based on the linear-quadratic regulator (LQR) problem, traffic-responsive urban control (TUC) [1] and its extensions (see [2], [3]) represent a multivariable feedback regulator approach for network-wide urban traffic control. Although TUC can deal with oversaturated conditions via minimizing and balancing the relative occupancies of network links, it may not be optimal for heterogeneous networks with multiple pockets of congestion. Inspired by the max pressure routing scheme for wireless networks, many local traffic control schemes have been proposed for networks of signalized intersections (see [4]–[7]), which involve evaluations at each intersection requiring information exclusively from adjacent links. Although the high accuracy of microscopic traffic models is desirable for simulation purposes, the increased model complexity results in complications for control, whereas local control strategies might not be able to operate properly under heavily congested conditions and fast propagation, as they do not protect the congested regions upstream. Another disadvantage of sophisticated local controllers is that they might require detailed information on traffic states, which is difficult to estimate or measure.

Literature on state estimation for road traffic focuses mainly on freeway networks: A mixture Kalman filter based on the cell transmission model is proposed in [8]. In [9], an extended Kalman filter is designed for real-time state and parameter estimation for a freeway network with dynamics described by the METANET model [10]. A particle filtering framework is proposed in [11] for a second order freeway traffic model that is efficiently parallelizable. Superiority of Lagrangian state estimation formulations over the Eulerian case using extended Kalman filters for the Lighthill-Whitham and Richards (LWR) model is reported in [12]. There is also some literature on urban traffic state estimation: In [13] an unscented Kalman filter is designed based on a kinematic wave model modified for urban traffic. An approach integrating the Kalman filter with advanced data fusion techniques is taken by [14] for urban network state estimation. A data fusion based extended Kalman filter is proposed in [15] for urban corridors based on the LWR model. Interestingly, even though there is considerable literature on traffic state estimation (especially for freeways), there are not many works on comparable techniques for large-scale urban networks. The majority of these works focus mainly on traffic state estimation, while how a proper estimation influences the performance of feedback controllers is not well studied, especially for large-scale urban networks.

An alternative to local traffic control methods is the hierarchical approach. A network-level controller optimizes network performance via macroscopic traffic flows through interregional actuation systems (e.g., perimeter control), whereas local controllers regulate microscopic traffic movements through intraregional actuation systems (e.g., signalized intersections). The macroscopic fundamental diagram (MFD) of urban traffic is a modeling tool for developing aggregated dynamic models of urban networks, which are required for the design of efficient network-level control schemes for the upper layer. It is possible to model an urban region with roughly homogeneous accumulation (i.e., small spatial link density heterogeneity) with an MFD, which provides a unimodal, low-scatter, and demand-insensitive relationship between accumulation and trip completion flow after a partitioning of the network into homogeneous regions (see [16] and [17]).

Isik Ilber Sirmatel and Nikolas Geroliminis are with the School of Architecture, Civil and Environmental Engineering, École Polytechnique Fédérale de Lausanne (EPFL), 1015 Lausanne, Switzerland. {isik.sirmatel,nikolas.geroliminis}@epfl.ch

MFD with an optimal accumulation was first proposed in [18], and its existence was recently verified with dynamic features and real data (see [19] and [20]). Analysis, modeling, and control methods for designing MFD-based traffic management schemes have been proposed by many researchers: Stability analysis [21], robust control [22], [23], proportional-integral control [24], [25], integration of agent-based modeling with MFD [26], hierarchical control [27], control via vehicle routing [28], [29], modeling of macroscopic flows considering link level capacity [30], optimal control [31]–[33], adaptive control [34], [35]. Application of the MPC technique to the control of urban networks with MFD modeling also attracted recent interest: Nonlinear MPC for a two-region network actuated with perimeter control [36], hybrid MPC with perimeter control and switching signal timing plans [37], dynamical modeling of heterogeneity and hierarchical control with MPC on the upper level [38], MPC with MFD-based travel time and delays as performance measures [39], multi-scale stochastic MPC with conventional and connected vehicles [40], two-level hierarchical MPC with MFD-based and link-level models [41], multimodal MFDs network model-based MPC of city-scale ride-sourcing systems [42], MPC with perimeter control and regional route guidance [43] and extensions with a path assignment mechanism [44]. A more detailed literature review of MFD-based modeling and control can be found in [45].

Most works in the literature on perimeter control assume that: a) Current values of accumulations $n_{ij}(t)$ and inflow demands $q_{ij}(t)$ (with i and j denoting the current and destination regions, respectively) are known (i.e., measured perfectly), b) future trajectories of inflow demands $q_{ij}(t)$ are available. Such assumptions are problematic for practice due to following reasons: 1) Measurements are corrupted by noise, 2) measuring $n_{ij}(t)$ or $q_{ij}(t)$ might be impossible, costly, or problematic due to privacy reasons, as they require information on the origins and destination of drivers, 3) assuming that future values of $q_{ij}(t)$ are known is unrealistic, as it is impossible to know OD demands exactly in advance. We address the first two shortcomings directly in this paper by a nonlinear moving horizon estimation (MHE) scheme. Employing a nonlinear dynamical model and past measurements to optimize over state trajectories in a finite horizon window, the MHE method specifies an advanced state estimation technique involving constrained nonlinear optimization. The method is integrated with a model predictive perimeter control scheme to provide a practicable traffic management framework, able to deal with cases of noisy measurements and lack of availability of information on $n_{ij}(t)$ and/or $q_{ij}(t)$. State estimation enables congestion management even in the case when measurements on the state are not available (i.e., when $n_{ij}(t)$ and $q_{ij}(t)$ are not measured) and improves control performance due to the filtering of noise from the measurements. An early version of this paper has been presented as [46].

II. Modeling

Consider a heterogeneous urban road network that can be partitioned into 2 homogeneous regions (see fig. 1). Each region i, with $i \in \{1,2\}$, has a well-defined outflow MFD

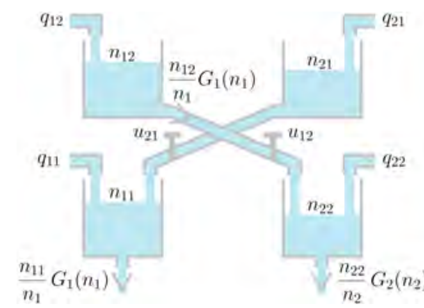

Fig. 1. Four reservoirs representation of an urban network with 2 regions.

$G_i(n_i(t))$ (veh/s), which is the outflow (i.e., trip completion flow) at accumulation $n_i(t)$. The flow of vehicles appearing in region i and demanding trips to destination j (i.e., origin-destination (OD) inflow demand) is $q_{ij}(t)$ (veh/s), whereas $n_{ij}(t)$ (veh) is the accumulation in region i with destination j, while $n_i(t)$ (veh) is the regional accumulation at time t; $n_i(t) = \sum_{j=1}^{2} n_{ij}(t)$. Between the two regions there exists perimeter control actuators $u_{12}(t)$ and $u_{21}(t) \in [u_{\min}, u_{\max}]$ (with $0 \leq u_{\min} < u_{\max} \leq 1$), that can restrict transfer flows. Dynamics of a 2-region MFDs network is [36]:

$$\dot{n}_{11}(t) = q_{11}(t) + M_{21}(t) - M_{11}(t) \tag{1a}$$
$$\dot{n}_{12}(t) = q_{12}(t) - M_{12}(t) \tag{1b}$$
$$\dot{n}_{21}(t) = q_{21}(t) - M_{21}(t) \tag{1c}$$
$$\dot{n}_{22}(t) = q_{22}(t) + M_{12}(t) - M_{22}(t), \tag{1d}$$

while $M_{ii}(t)$ and $M_{ij}(t)$ express the exit (i.e., vehicles disappearing from the network) and transfer flows (i.e., vehicles transferring between regions), respectively:

$$M_{ii}(t) = \frac{n_{ii}(t)}{n_i(t)} G_i(n_i(t)) \quad \forall i \in \{1,2\} \tag{2a}$$
$$M_{ij}(t) = u_{ij}(t) \frac{n_{ij}(t)}{n_i(t)} G_i(n_i(t)) \quad \forall i \in \{1,2\},\ j \neq i. \tag{2b}$$

It is important to note here that the above expressions for $M_{ii}(t)$ and $M_{ij}(t)$ involve approximating the outflow MFD $G_i(n_i(t))$ as the ratio of a production MFD $P_i(n_i(t))$ (veh.m/s) and a regional average trip length l_i (m) (that is assumed to be constant and OD-independent). Accumulation-based models can be improved using flows involving OD-dependent trip lengths, which can be done, e.g., by rewriting eq. (2b) as follows:

$$M_{ij}(t) = \frac{n_{ii}(t)}{n_i(t)} \frac{P_i(n_i(t))}{l_{ij}}, \tag{3}$$

where l_{ij} (m) is the average trip length traveled inside region i for trips from i to j. Details of such models (and their extensions) can be found in [45] and [38]. In [19] the assumption of outflow being approximately equal to production divided by trip length was tested with real data without any OD information. Although the $P_i(n_i(t))/l_i$ approximation for outflow yields accumulation-based models that are adequate for control design with simplified system dynamics without delays, it should not be considered as a universal law. For example, strong demand fluctuations forming fast evolving transients can affect the distribution of trip lengths in a region at a specific time, possibly creating inaccuracies in $P_i(n_i(t))/l_i$ approximation of outflow.

All trips inside a region are assumed to have similar trip lengths (i.e., the origin and destination of the trip does not affect the distance traveled by a vehicle). Simulation and empirical results [19] suggest the possibility of approximating the MFD by an asymmetric unimodal curve skewed to the right (i.e., the critical accumulation n_i^{cr}, for which $G_i(n_i(t))$ is at maximum, is less than half of the jam accumulation n_i^{jam} that puts the region in gridlock). Thus, $G_i(n_i(t))$ can be expressed using a third degree polynomial in $n_i(t)$:

$$G_i(n_i(t)) = a_i n_i^3(t) + b_i n_i^2(t) + c_i n_i(t), \tag{4}$$

where a_i, b_i, and c_i are known parameters (which are to be extracted from historical data in practice). Multi-region dynamical modeling formulations for urban networks with more than two regions can be found in [38], [43].

III. Optimal Estimation and Control

A. Modeling for Demand Estimation

Obtaining accurate real-time information on inflow demands $q_{ij}(t)$ is difficult in practice; such measurements are either unavailable or highly noisy. Circumventing this problem is possible through including inflow demands in the state estimation procedure. Towards this end we define the inflow demand terms $q_{ij}(t)$ as state variables, yielding the augmented dynamical system:

$$\begin{bmatrix} \dot{n}(t) \\ \dot{u}(t) \\ \dot{q}(t) \end{bmatrix} = \begin{bmatrix} f_n(n(t), q(t), u(t)) \\ \delta(t) \\ \mathbf{0} \end{bmatrix}, \tag{5}$$

where $n(t)$ contains the accumulations $n_{ij}(t)$

$$n(t) = [n_{11}(t)\ n_{12}(t)\ n_{21}(t)\ n_{22}(t)]^{\text{T}}, \tag{6}$$

$q(t)$ contains the inflow demands $q_{ij}(t)$

$$q(t) = [q_{11}(t)\ q_{12}(t)\ q_{21}(t)\ q_{22}(t)]^{\text{T}}, \tag{7}$$

$u(t)$ contains the perimeter controls

$$u(t) = [u_{12}(t)\ u_{21}(t)]^{\text{T}}, \tag{8}$$

whereas $f_n(\cdot)$ is the dynamics given in eq. (1), while $\mathbf{0}$ is a vector of zeros (expressing that the inflow demands are assumed to be constant in time).

Note that, to facilitate formulations related to state estimation, the perimeter controls $u_{12}(t)$ and $u_{21}(t)$ are defined here as state variables, with the actual control input vector being $\delta(t) = [\delta_{12}(t)\ \delta_{21}(t)]^{\text{T}}$. The reason is that, state estimation is assumed to be conducted before computing the control input, thus during state estimation at time step t it is impossible to access $u(t)$ as it is not available yet.

Considering additive process noise $w(t)$, and measurements $y(t)$ corrupted by noise $v(t)$, we can write the dynamics and measurement as:

$$\dot{x}(t) = f(x(t), \delta(t)) + w(t) \tag{9}$$

$$y(t) = h(x(t)) + v(t), \tag{10}$$

where $x(t)$ is the augmented state

$$x(t) = [n(t)^{\text{T}}\ u(t)^{\text{T}}\ q(t)^{\text{T}}]^{\text{T}}, \tag{11}$$

$f(\cdot)$ is the augmented dynamical system given in eq. (5), $h(\cdot)$ is the measurement equation, while $w(t)$ contains unknown disturbances (i.e., process noise) expressing plant-model mismatch:

$$\begin{gathered} w(t) = [w_n(t)^{\text{T}}\ \mathbf{0}^{\text{T}}]^{\text{T}} \\ w_n(t) = [w_{n_{11}}(t)\ w_{n_{12}}(t)\ w_{n_{21}}(t)\ w_{n_{22}}(t)]^{\text{T}}, \end{gathered} \tag{12}$$

where $w_{n_{ij}}(t) \sim \mathcal{N}(0, \sigma^2_{w,n})$ is white Gaussian noise, modeling uncertainty in the dynamics $f_n(\cdot)$. As the inflow demands are modeled as constant parameters, their dynamics are assumed to be unaffected by process noise, whereas perimeter controls are directly manipulated by the controller without any associated uncertainty, thus these two terms have their associated process noise terms equal to 0.

B. Measurement Configurations

Measurements available in an application dictate which state variables can be included in the dynamical model that is used to design model-based estimation and control schemes. In this section we present some measurement configurations likely to be encountered in practice of large-scale urban road network management. The important question of whether the traffic state can be determined from available measurements (i.e., observability) will be tackled in the next section.

1) Measurements on Accumulations $n_{ij}(t)$: One straightforward measurement configuration involves simply measuring all accumulations $n_{ij}(t)$:

$$\begin{gathered} y_\alpha(t) = h_\alpha(x(t)) + v_\alpha(t) \\ h_\alpha(x(t)) = n(t) \\ v_\alpha(t) = [v_{n_{11}}(t)\ v_{n_{12}}(t)\ v_{n_{21}}(t)\ v_{n_{22}}(t)]^{\text{T}}, \end{gathered} \tag{13}$$

where $v_{n_{ij}}(t) \sim \mathcal{N}(0, \sigma^2_{v,n_{ij}})$ is white Gaussian noise, modeling measurement noise of $n_{ij}(t)$. While in most works on MFD-based control it is assumed that measurements on $n_{ij}(t)$ are available, this might be difficult in practice with conventional sensors, since measuring $n_{ij}(t)$ requires drivers to report their destination at the start of the trip.

2) Measurement on Regional Accumulations $n_i(t)$ and Transfer Flows $M_{ij}(t)$: Compared to $n_{ij}(t)$, regional accumulations $n_i(t)$ and transfer flows $M_{ij}(t)$ are easier to measure as they require loop detectors only (dispersed inside a region for $n_i(t)$ and placed at the boundary between regions for $M_{ij}(t)$). Thus, a more practical measurement configuration involves measuring $M_{ij}(t)$ and $n_i(t)$:

$$\begin{gathered} y_\beta(t) = h_\beta(x(t)) + v_\beta(t) \\ h_\beta(x(t)) = [n_1(t)\ n_2(t)\ M_{12}(t)\ M_{21}(t)]^{\text{T}} \\ v_\beta(t) = [v_{n_1}(t)\ v_{n_2}(t)\ v_{M_{12}}(t)\ \ v_{M_{21}}(t)]^{\text{T}}, \end{gathered} \tag{14}$$

where $v_{n_i}(t) \sim \mathcal{N}(0, \sigma^2_{v,n_i})$ and $v_{M_{ij}}(t) \sim \mathcal{N}(0, \sigma^2_{v,M_{ij}})$ are white Gaussian noise terms, modeling measurement noise of $n_i(t)$ and $M_{ij}(t)$, respectively.

3) Measurements on Inflow Demands $q_{ij}(t)$: In some well-instrumented applications it might be possible to measure all $q_{ij}(t)$ terms:

$$\begin{aligned} y_\gamma(t) &= h_\gamma(x(t)) + v_\gamma(t) \\ h_\gamma(x(t)) &= q(t) \\ v_\gamma(t) &= v_q(t), \end{aligned} \tag{15}$$

where $v_\gamma(t)$ is the noise associated with $q_{ij}(t)$:

$$v_q(t) = [v_{q_{11}}(t)\ v_{q_{12}}(t)\ v_{q_{21}}(t)\ v_{q_{22}}(t)]^{\mathrm{T}}, \tag{16}$$

where $v_{q_{ij}}(t) \sim \mathcal{N}(0, \sigma^2_{v_q})$ is white Gaussian noise, modeling measurement noise of $q_{ij}(t)$.

4) Measurements on Regional Inflow Demands $q_i(t)$: Some applications might involve access to measurements on $q_i(t)$ instead of $q_{ij}(t)$ (e.g., when GPS information is collected for a sample of vehicles):

$$\begin{aligned} y_\zeta(t) &= h_\zeta(x(t)) + v_\zeta(t) \\ h_\zeta(x(t)) &= \begin{bmatrix} q_{11}(t) + q_{12}(t) \\ q_{21}(t) + q_{22}(t) \end{bmatrix} \quad v_\zeta(t) = \begin{bmatrix} v_{q_1}(t) \\ v_{q_2}(t) \end{bmatrix}, \end{aligned} \tag{17}$$

where $v_{q_i}(t) \sim \mathcal{N}(0, \sigma^2_{v,q_i})$ is white Gaussian noise, modeling measurement noise of $q_i(t)$.

C. Measurement Compositions and Observability Test

Availability of measurements affects the possibility of observing the system state, which is related to the observability property of a dynamical system. Roughly stated, observability is about whether the state can be uniquely determined based on the measurements or not. A dynamical system (i.e., $f(\cdot)$ and $h(\cdot)$) has to be observable in order to do estimation. Observability of nonlinear systems can be checked using the *observability rank condition* developed in [47]. For affine-input systems (such as eq. (5)), which can be written as:

$$\begin{aligned} \dot{x}(t) &= f(x) + \sum_{j=1}^{m} g_j(x(t)) u_j(t) \\ y_i(t) &= h_i(x(t)),\ i = 1, \ldots, p, \end{aligned}$$

where $x \in \mathbb{R}^l$ is the state, $u_j \in \mathbb{R}$ (with $j = 1, \ldots, m$) are control inputs, and $y_i \in \mathbb{R}$ (with $i = 1, \ldots, p$) are the measurements, it is possible to use a simpler form of the rank condition, as included in the software package developed in [48] or presented in an algorithm given in [49]. This observability test involves constructing the *observability codistribution* [48]:

$$\Omega_O = \langle f, g_1, \ldots, g_m \mid \mathrm{span}\{dh_1, \ldots, dh_p\} \rangle, \tag{18}$$

and checking its rank. If the rank of Ω_O is equal to l (i.e., dimension of the state x), then the observability rank condition is satisfied [48], [49], indicating that the system is locally weakly observable (see §3 in [47] for details).

To check observability of the two-region MFD-based urban network dynamics, we conducted tests for four measurement compositions based on the configurations given earlier:

$$\begin{aligned} h_1(x(t)) &= \begin{bmatrix} h_\alpha(x(t)) \\ h_\gamma(x(t)) \\ u(t) \end{bmatrix} \quad h_2(x(t)) = \begin{bmatrix} h_\alpha(x(t)) \\ h_\zeta(x(t)) \\ u(t) \end{bmatrix} \\ h_3(x(t)) &= \begin{bmatrix} h_\beta(x(t)) \\ h_\gamma(x(t)) \\ u(t) \end{bmatrix} \quad h_4(x(t)) = \begin{bmatrix} h_\beta(x(t)) \\ h_\zeta(x(t)) \\ u(t) \end{bmatrix}, \end{aligned} \tag{19}$$

where the compositions are: a) h_1 (with accumulations $n_{ij}(t)$ and inflow demands $q_{ij}(t)$), b) h_2 (with accumulations $n_{ij}(t)$ and regional inflow demands $q_i(t)$), c) h_3 (with regional accumulations $n_i(t)$, transfer flows $M_{ij}(t)$, and inflow demands $q_{ij}(t)$), d) h_4 (with regional accumulations $n_i(t)$, transfer flows $M_{ij}(t)$, and regional inflow demands $q_i(t)$). Note that the perimeter controls $u(t)$ are included in all compositions; they are known and thus need not be measured. Observability tests are done using the ProPac package [48] of the computer algebra tool Mathematica, where observability rank condition is checked for the dynamics eq. (5) and each measurement composition. In all four cases the observability rank condition is satisfied according to the results obtained from ProPac.

Since measurement configurations involving limited (i.e., h_2 and h_3) or no OD-based information (i.e., h_4) still yield observability, it is possible to design state estimators to reconstruct $n_{ij}(t)$ and $q_{ij}(t)$ from measurements. Deployment of traffic control schemes involving feedback on $n_{ij}(t)$ and $q_{ij}(t)$ is thus possible with state estimation even if these cannot be measured. This has important implications for practice, since $n_{ij}(t)$ and $q_{ij}(t)$ are difficult to measure.

D. Moving Horizon Estimation

We formulate the problem of finding state estimate trajectories for a moving time horizon extending a fixed length into the past, striking a trade-off between measurements and the prediction model, as the following nonlinear MHE problem:

$$\begin{aligned} \underset{w_k}{\text{minimize}} \quad & \sum_{k=-N_\mathrm{e}}^{-1} \|w_k\|_Q^2 + \sum_{k=-N_\mathrm{e}}^{0} \|v_k\|_R^2 \\ \text{subject to} \quad & \text{for } k = -N_\mathrm{e}, \ldots, 0 : \\ & \quad v_k = y_{t+k}(t) - h(x_k) \\ & \text{for } k = -N_\mathrm{e}, \ldots, -1 : \\ & \quad x_{k+1} = F(x_k, \delta_{t+k}(t), T_\mathrm{e}) + w_k \\ & \text{for } k = 1, \ldots, N_\mathrm{e} : \\ & \quad \text{a) } 0 \le n_{ij,k} \quad \forall i, j \in \{1, 2\} \\ & \quad \text{b) } n_{i,k} \le n_{i,\mathrm{jam}} \quad \forall i \in \{1, 2\} \\ & \quad \text{c) } 0 \le q_{ij,k} \le \bar{q}_{ij} \quad \forall i, j \in \{1, 2\}, \end{aligned} \tag{20}$$

where k is the time interval counter internal to the MHE, N_e is the horizon of the MHE (i.e., estimation horizon), t is the current time step, Q and R are weighting matrices on the process and measurement noise, respectively, w_k, v_k, and x_k are the process noise, measurement noise, and state vectors, for the time interval k, respectively, $h(\cdot)$ is the measurement equation (one of the four given in eq. (19)), F is the discrete-time version of the dynamics given in eq. (9) with MHE sampling time T_{e}, whereas $\{y_{t+k}(t)\}_{k=-N_{\mathrm{e}}}^{0}$ and $\{\delta_{t+k}(t)\}_{k=-N_{\mathrm{e}}}^{-1}$ are past measurement and control input trajectories available at time step t, respectively, while $n_{ij,k}$, $n_{i,k}$, and $q_{ij,k}$ are the accumulation, regional accumulation, and inflow demand state variables internal to the MHE, respectively, with the constraints expressing their physical or known limits: a) accumulations are non-negative, b) regional accumulations cannot exceed jam accumulation, c) inflow demands are non-negative and cannot exceed some known upper bound $\bar{q}_{ij}$.

E. Model Predictive Control

We formulate the problem of finding the control inputs that minimize total time spent (TTS) for a finite horizon as the following economic nonlinear MPC problem (based on [36]):

$$\begin{aligned}
\underset{\delta_k}{\text{minimize}} \quad & T \cdot \sum_{k=0}^{N_{\mathrm{c}}} \sum_{i=1}^{2} \sum_{j=1}^{2} n_{ij,k} \qquad (21)\\
\text{subject to} \quad & n_0 = \hat{n}_t(t) \\
& u_0 = u(t - T_{\mathrm{c}}) \\
& |\delta_0| \leq \Delta_u \\
& \text{for } k = 0, \ldots, N_{\mathrm{c}} - 1 : \\
& \quad n_{k+1} = F_n(n_k, \hat{q}_t(t), u_k, T_{\mathrm{c}}) \\
& \quad u_{k+1} = F_u(\delta_k, T_{\mathrm{c}}) \\
& \quad u_{\min} \leq u_k \leq u_{\max} \\
& \text{for } k = 1, \ldots, N_{\mathrm{c}} : \\
& \quad 0 \leq n_{ij,k} \quad \forall i \in \{1, 2\} \\
& \quad \sum_{j=1}^{2} n_{ij,k} \leq n_{i,\mathrm{jam}} \quad \forall i \in \{1, 2\},
\end{aligned}$$

where k is the time interval counter internal to the MPC, N_{c} is the horizon of the MPC (i.e., prediction horizon), $\hat{n}_t(t)$ and $\hat{q}_t(t)$ are the information (either measured or estimated) available at time step t on the states $n(t)$ and $q(t)$ (with t being the current time step), Δ_u is the rate limiting parameter on control inputs, n_k, u_k, and δ_k, the accumulation state, perimeter control state, and control input vectors internal to the MPC, respectively, F_n and F_u are the discrete-time version of the corresponding dynamics given in eq. (5) with MPC sampling time T_{c}, whereas $n_{ij,k}$ and $n_{i,k}$ are the accumulation and regional accumulation state variables internal to the MPC. Note that future inflow demands for the prediction horizon are assumed to be constant and fixed to their estimated value. This assumption is analyzed in a later section.

The optimization problems given in eqs. (20) and (21) are nonconvex nonlinear programs, which can be solved efficiently via, e.g., sequential quadratic programming or interior point solvers (for details, see [50]).

F. Integrated State Estimation and Control

For the combined state estimation and perimeter control of large-scale urban networks, we propose a traffic management scheme integrating MHE and MPC, given in eqs. (20) and (21). Operation of the scheme is formalized in algorithm 1. We are interested in investigating how measurement errors, types of measurement and quality of estimation (or even no estimation) influence performance of the MFD-based controllers. This is clearly an important aspect that deserves investigation before moving to field applications of MFD-based control.

Algorithm 1 Operation of state estimation and control.

At plant time step $t_{\mathrm{p}} = 0$, initialize simulation from $x(0)$.

1) At each MHE time step t_{e} (with $t_{\mathrm{e}} \in T_{\mathrm{e}} \cdot \mathbb{Z}_{\geq 0}$), given past measurements $\{y(t_{\mathrm{e}} - k)\}_{k=N_{\mathrm{e}}}^{0}$ and control inputs $\{\delta(t_{\mathrm{e}} - k)\}_{k=N_{\mathrm{e}}}^{1}$, solve the MHE problem (20) to obtain the state estimates $\{\hat{x}_{t_{\mathrm{e}}-k}(t_{\mathrm{e}})\}_{k=N_{\mathrm{e}}}^{0}$.
2) At each MPC time step t_{c} (with $t_{\mathrm{c}} \in T_{\mathrm{c}} \cdot \mathbb{Z}_{\geq 0}$), given the most current state estimate $\hat{x}_{t_{\mathrm{c}}}(t_{\mathrm{c}})$, solve the MPC problem (21) to obtain control inputs $\{\delta_{t_{\mathrm{c}}+k}(t_{\mathrm{c}})\}_{k=0}^{N_{\mathrm{c}}-1}$.
3) At each plant time step t_{p} (with $t_{\mathrm{p}} \in T_{\mathrm{p}} \cdot \mathbb{Z}_{\geq 0}$), apply the most current control input $\delta_{t_{\mathrm{c}}}(t_{\mathrm{c}})$ (with $t_{\mathrm{c}} \leq t_{\mathrm{p}}$) to the plant; if simulating, evolve system dynamics given in eq. (5) discretized in time with plant sampling time T_{p}.

Repeat steps 1, 2, and 3 for $t_{\mathrm{p}} \in T_{\mathrm{p}} \cdot \mathbb{Z}_{\geq 0}$ up to t_{final}.

IV. Simulation Results

A. Congested Scenario

All simulations are conducted on a 2-region urban network with the simulation model given in eq. (9) for representing the reality. The regions have the same MFD, with the parameters $a_i = 4.133 \cdot 10^{-11}$, $b_i = -8.282 \cdot 10^{-7}$, $c_i = 0.0042$, jam accumulation $n_{i,\mathrm{jam}} = 10^4$ (veh), critical accumulation $n_{i,\mathrm{cr}} = 3.4 \cdot 10^3$ (veh), maximum outflow $G(n_{i,\mathrm{cr}}) = 6.3$ (veh/s), for $i = \{1, 2\}$, which are consistent with the MFD observed in a part of downtown Yokohama (see [19]).

The dynamics are discretized with the Runge–Kutta method with a plant sampling time of $T_{\mathrm{p}} = 5$ s for simulation, while the sampling times of estimation and control are $T_{\mathrm{e}} = 10$ s and $T_{\mathrm{c}} = 90$ s, respectively (with the control sampling time reflecting a realistic value for traffic light cycle time). The MHE and MPC schemes are built using direct multiple shooting [51], while implementation is done using MPCTools [52], which is an interface to CasADi [53], with IPOPT [54] as solver, in MATLAB 8.5.0 (R2015a), on a 64-bit Windows PC with 3.6-GHz Intel Core i7 processor and 16-GB RAM. Horizons MHE and MPC are both chosen as 30 minutes, following the MPC tuning results [36]. Tuning for MHE is given in a later section. The perimeter controls are bounded as $0.1 \leq u_{ij}(t) \leq 0.9$, with a rate limit of $\Delta_u = 0.1$. Simulation length is $t_{\mathrm{final}} = 240$ minutes.

Standard deviations of the process and measurement noise are chosen as $\sigma_{w,n} = 0.5$ veh/s, $\sigma_{v,n_{ij}} = 1000$ veh, $\sigma_{v,q_{ij}} = 0.5$ veh/s, $\sigma_{v,n_i} = 1000$ veh, $\sigma_{v,M_{ij}} = 1$ veh/s, $\sigma_{v,q_i} = 0.5$ veh/s, specifying severe measurement and process noise conditions. Weighting matrices of the MHE (i.e., Q and R) contain the inverses of these values, to reflect the fact that the stage cost terms related to the process and measurement noises should be weighted inversely proportional to the associated amount of uncertainty (that is, e.g., the measurements should be trusted more if the measurement noise has a lower variance).

Control performance is evaluated using average time spent per vehicle (TSPV), defined for a single experiment as:

$$\text{TSPV} = \sum_{t=1}^{t_{\text{final}}} \sum_{i=1}^{2} \sum_{j=1}^{2} \frac{n_{ij}(t)}{q_{ij}(t)}, \tag{22}$$

while for estimation performance we define two metrics based on the root-mean-square estimation error, one for $n_{ij}(t)$ and the other for $q_{ij}(t)$:

$$\text{RMSE}_n = \frac{1}{4} \sum_{i=1}^{2} \sum_{j=1}^{2} \sqrt{\frac{\sum_{t=1}^{t_{\text{final}}} (n_{ij}(t) - \hat{n}_{ij}(t))^2}{t_{\text{final}}}} \tag{23}$$

$$\text{RMSE}_q = \frac{1}{4} \sum_{i=1}^{2} \sum_{j=1}^{2} \sqrt{\frac{\sum_{t=1}^{t_{\text{final}}} (q_{ij}(t) - \hat{q}_{ij}(t))^2}{t_{\text{final}}}} \tag{24}$$

where $\hat{n}_{ij}(t)$ and $\hat{q}_{ij}(t)$ are the estimates computed by the MHE at time t, for $n_{ij}(t)$ and $q_{ij}(t)$, respectively.

In the congested scenario, the network is uncongested at the beginning, but faces increased inflow demands as time progresses. For the four measurement compositions with the proposed MHE-MPC method (with inflow demands fixed to their estimated values at time t for the prediction horizon of the MPC), the results are given in figs. 2–6, which contain the true, estimated, and when applicable, measured trajectories of accumulations $n_{ij}(t)$, inflow demands $q_{ij}(t)$, regional accumulations $n_i(t)$, transfer flows $M_{ij}(t)$, and regional inflow demands $q_i(t)$, true trajectories of regional accumulations $n_i(t)$, regional outflows $G_i(t)$, trip completion flows $M_{ii}(t)$, and perimeter controls $u_{ij}(t)$, together with the active parts of the outflow MFDs. A summary of more detailed results is given in table I, which shows control and estimation performance metrics together with CPU times for the MHE and MPC, for the four measurement composition cases comparing an extended Kalman filter (EKF) with the proposed MHE method (both using MPC as the controller), together with a no control case (with perimeter controls fixed to their maximum value of 0.9), and a y-MPC case representing MPC directly using measurements of $n_{ij}(t)$ (i.e., without state estimation).

The results in figs. 2–6 suggest that the proposed MHE-MPC scheme is successful in managing congestion even under severe noise conditions with measurements having partial information (i.e., h_2, h_3, and h_4, given in eq. (19)). For the h_1 case depicted in fig. 2, despite the significant measurement noise present in both in $q_{ij}(t)$ and $n_{ij}(t)$ (with $\sigma_{v,q_{ij}} = 0.5$ veh/s and $\sigma_{v,n_{ij}} = 1000$ veh), the estimation errors are small resulting in high control performance. From the y-MPC results (i.e., MPC without MHE) in figures (i) and (j) in fig. 2, it can be observed that without estimation the network reaches congested states and there is a significant loss of capacity for region. This is evidenced also by the network experiencing near-gridlock conditions for the no control (in region 1) and y-MPC (in region 2) cases, as can be seen in fig. 6. This indicates the importance of estimation for high performance congestion management. Interestingly, as seen from figures (i) and (l) in fig. 2, the MPC decides to let region 2 reach congested states before restricting flows by decreasing u_{12}. This highlights that due to the high level of complexity of urban networks, standard and simple control approaches (e.g., keeping the city center at the critical accumulation) might have counter-productive or non-intuitive results with worse performance. Similar conclusions can be drawn for the control actions for measurement types h_2 to h_4 as shown in figs. 3–5. From fig. 3 it can be seen for h_2 that since $q_{ij}(t)$ is not measured, there is clearly higher error in the estimation of $q_{ij}(t)$ compared to the h_1 case (where $q_{ij}(t)$ are measured). Nevertheless, the control performance is similar quality, as $n_{ij}(t)$ and $n_{ij}(t)$ are estimated with a level of accuracy similar to h_1. An interesting observation based on fig. 5 is that even with the very limited information present in h_4 involving only $n_i(t)$, $M_{ij}(t)$, and $q_i(t)$ measurements, it is still possible to estimate $n_{ij}(t)$ with high accuracy, and despite the increased estimation errors in $q_{ij}(t)$, the control performance is similar to h_1. Overall, the results indicate substantial potential towards real-world implementation of model predictive perimeter control schemes, where OD-based information and future demands might be unavailable and measurements might be corrupted with large amounts of noise. Furthermore, from the results in table I it can be observed that while EKF performance (both estimation and control) suffers from measurement compositions with limited information (i.e., especially h_2 and h_4), MHE seems to be insensitive to the effects of limited information. Furthermore, the results indicate real-time feasibility of the MHE and MPC schemes, as their CPU times of about 1.2 and 0.5 seconds are roughly negligible compared to their sampling times of 10 and 90 seconds, respectively. It is important to note here that a direct quantitative comparison between the four measurement compositions is impossible simply because they involve different measurements, the noise levels of which are not comparable. We also tested accumulation-based models using eq. (3), the results of which are omitted since they yielded results similar to those presented here.

TABLE I
PERFORMANCE EVALUATION FOR CONGESTED SCENARIO

meas. comp. - st. est.	TSPV (min)	RMSE_n (veh)	RMSE_q (veh/s)	mean/max CPU time MHE (s)	mean/max CPU time MPC (s)
no control	26.1	-	-	-	-
y-MPC	20.8	-	-	-	0.30/0.41
h_1-EKF	18.7	349.1	0.80	-	0.32/0.47
h_1-MHE	18.4	228.7	0.75	0.72/1.13	0.33/0.46
h_2-EKF	18.8	584.2	1.24	-	0.31/0.44
h_2-MHE	18.1	265.8	0.89	0.75/1.19	0.33/0.46
h_3-EKF	18.3	318.9	0.80	-	0.32/0.47
h_3-MHE	18.1	218.0	0.75	0.75/1.19	0.33/0.46
h_4-EKF	18.7	583.6	1.11	-	0.31/0.43
h_4-MHE	17.7	277.4	0.91	0.80/1.22	0.33/0.50

B. Sensitivity to Measurement Noise Intensity

Changing measurement noise intensity is expected to affect estimation and control performance. This effect is examined by a sensitivity analysis, where a set of 50 randomly generated scenarios (each with a different inflow demand profile with

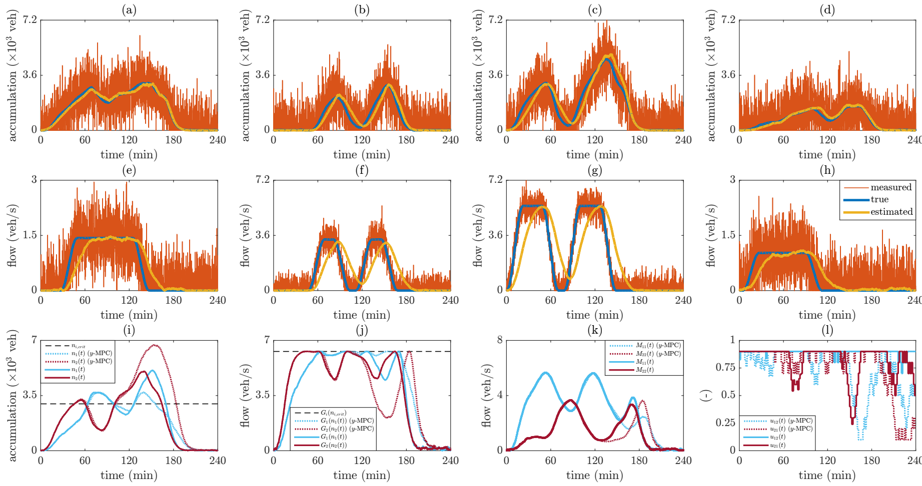

Fig. 2. Results of the congested scenario using h_1 with the combined MHE-MPC scheme: Accumulations (a) $n_{11}(t)$, (b) $n_{12}(t)$, (c) $n_{21}(t)$, (d) $n_{22}(t)$; inflow demands (e) $q_{11}(t)$, (f) $q_{12}(t)$, (g) $q_{21}(t)$, (h) $q_{22}(t)$; regional accumulations (i) $n_1(t)$ and $n_2(t)$; regional outflows (j) $G_1(n_1(t))$ and $G_2(n_2(t))$; trip completion flows (k) $M_{11}(t)$ and $M_{22}(t)$; perimeter controls (l) $u_{12}(t)$ and $u_{21}(t)$, with dashed lines in (i) to (l) denoting y-MPC results.

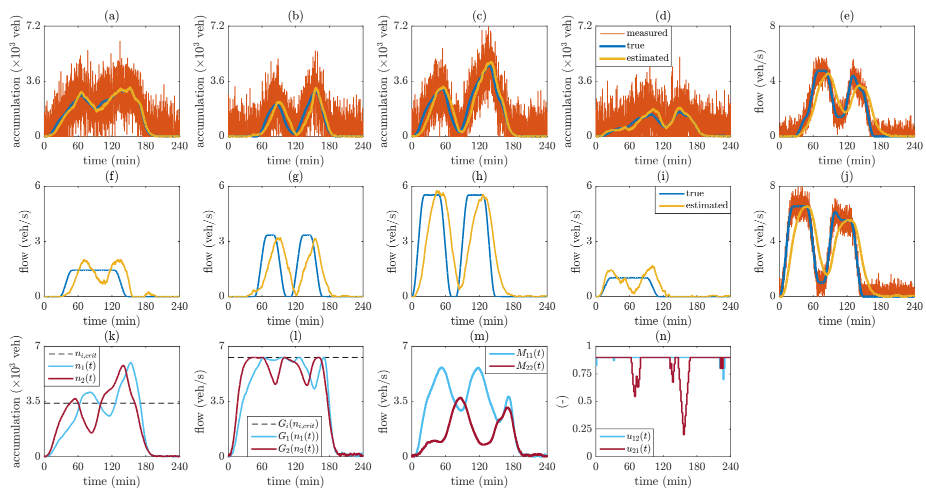

Fig. 3. Results of the congested scenario using h_2 with the combined MHE-MPC scheme: Accumulations (a) $n_{11}(t)$, (b) $n_{12}(t)$, (c) $n_{21}(t)$, (d) $n_{22}(t)$; regional inflow demands (e) $q_1(t)$, (j) $q_2(t)$; inflow demands (f) $q_{11}(t)$, (g) $q_{12}(t)$, (h) $q_{21}(t)$, (i) $q_{22}(t)$; regional accumulations (k) $n_1(t)$ and $n_2(t)$; regional outflows (l) $G_1(n_1(t))$ and $G_2(n_2(t))$; trip completion flows (m) $M_{11}(t)$ and $M_{22}(t)$; perimeter controls (n) $u_{12}(t)$ and $u_{21}(t)$.

moderate to high demands) is tested under the same conditions with the congested scenario (with the exception of sampling times, which are all chosen as 90), varying only the standard deviations of measurement noise: $\sigma_{v,n_{ij}}$ from 100 veh to 1000 veh for the h_1 and h_2 cases; σ_{v,n_i} from 100 veh to 1000 veh and $\sigma_{v,M_{ij}}$ from 0.1 veh/s to 1 veh/s (σ_{v,n_i} and $\sigma_{v,M_{ij}}$ changed together) for h_3 and h_4.

The results are shown in figs. 7–9, depicting RMSE$_n$, RMSE$_q$, and TSPV, respectively, as a function the measurement noise standard deviations. As expected, the results suggest degradation in estimation performance with increasing noise levels. Inflow demand estimation performance (i.e., RMSE$_q$), for the cases of h_1 and h_3, seems to be insensitive to increasing noise levels, which can be attributed to the fact that the inflow demands $q_{ij}(t)$ are measured directly in these two cases, which (unlike the cases of h_2 and h_4) do not rely on the rest of the measurements for reconstructing the inflow demands. Furthermore, it can be observed that for all metrics the MHE is much less sensitive to changes in noise levels compared to the EKF. This is especially pronounced for the TSPV metric, where MHE is almost completely insensitive to increasing noise for all measurement compositions, while the EKF shows substantial degradations for the cases of h_2 and h_4. This can be attributed to features of MHE: (a) it employs a nonlinear model directly (i.e., without any approximations, as in the case of linearization in EKF), (2) it optimizes over state trajectories considering known measurement trajectories inside a finite horizon window into the past (while EKF uses only the last measurement), (3) unlike EKF, it can handle state constraints systematically (see [55] for a detailed discussion comparing MHE and EKF).

C. Sensitivity of Control Performance to Noisy Measurements without State Estimation

Deploying controllers using noisy measurements without state estimators is expected to have adverse affects on control

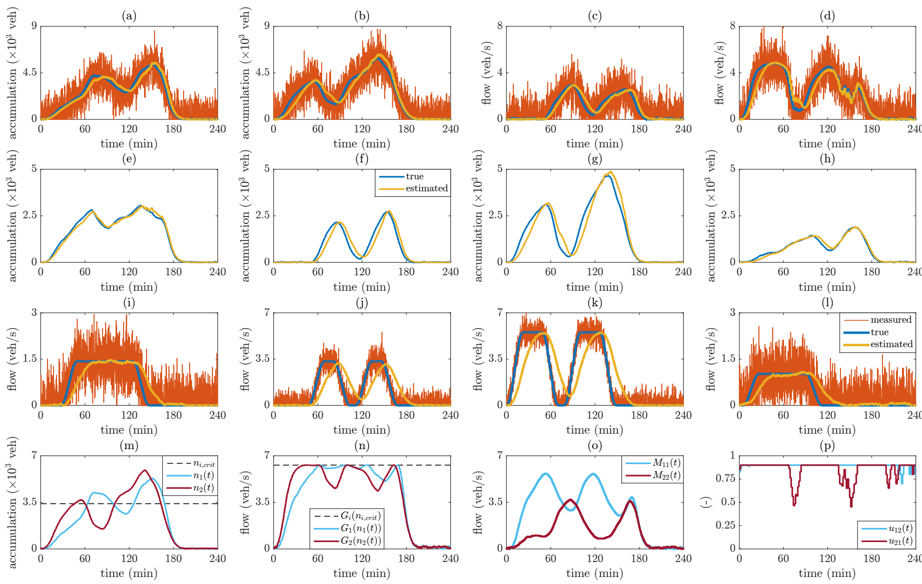

Fig. 4. Results of the congested scenario using h_3 with the combined MHE-MPC scheme: Regional accumulations (a) $n_1(t)$, (b) $n_2(t)$; transfer flows (c) $M_{12}(t)$, (d) $M_{21}(t)$; accumulations (e) $n_{11}(t)$, (f) $n_{12}(t)$, (g) $n_{21}(t)$, (h) $n_{22}(t)$; inflow demands (i) $q_{11}(t)$, (j) $q_{12}(t)$, (k) $q_{21}(t)$, (l) $q_{22}(t)$; regional accumulations (m) $n_1(t)$ and $n_2(t)$; regional outflows (n) $G_1(n_1(t))$ and $G_2(n_2(t))$; trip completion flows (o) $M_{11}(t)$ and $M_{22}(t)$; perimeter controls (p) $u_{12}(t)$ and $u_{21}(t)$.

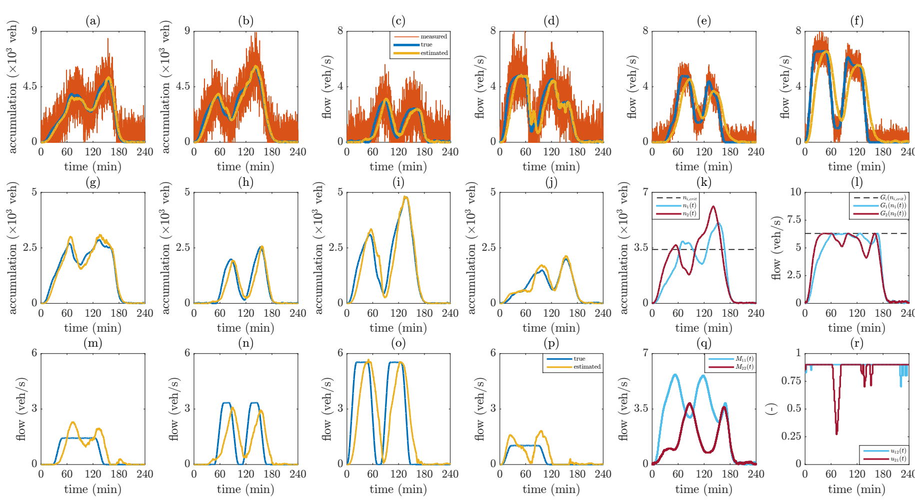

Fig. 5. Results of the congested scenario using h_4 with the combined MHE-MPC scheme: Regional accumulations (a) $n_1(t)$, (b) $n_2(t)$; transfer flows (c) $M_{12}(t)$, (d) $M_{21}(t)$; regional inflow demands (e) $q_1(t)$, (f) $q_2(t)$; accumulations (g) $n_{11}(t)$, (h) $n_{12}(t)$, (i) $n_{21}(t)$, (j) $n_{22}(t)$; regional accumulations (k) $n_1(t)$ and $n_2(t)$; regional outflows (l) $G_1(n_1(t))$ and $G_2(n_2(t))$; inflow demands (m) $q_{11}(t)$, (n) $q_{12}(t)$, (o) $q_{21}(t)$, (p) $q_{22}(t)$; trip completion flows (q) $M_{11}(t)$ and $M_{22}(t)$; perimeter controls (r) $u_{12}(t)$ and $u_{21}(t)$.

performance, since the controller has to rely on information with a large amount of corruption by noise. To further investigate this point a sensitivity analysis is performed, where a set of 50 randomly generated scenarios (each with a different inflow demand profile with high demands) is tested under the same conditions with the congested scenario, varying only the standard deviations of measurement noise ($\sigma_{v,n_{ij}}$ from 100 veh to 1000 veh). The results of an MPC scheme directly using the measurements (i.e., y-MPC) are compared with MPC schemes using EKF and MHE as state estimator, with the h_1 measurement composition. This is done for fair comparison since y-MPC requires the h_1 measurement composition as it does not have access to a state estimator or observer to extract the state from the measurement.

The results are shown in fig. 10, depicting TSPV and improvement in TSPV, respectively, as a function $\sigma_{v,n_{ij}}$. As expected, without a state estimator to filter out noise in the measurement, the control performance shows severe degradations with increasing levels of noise. However, using the EKF or MHE, it is possible to keep control performance insensitive to mesurement noise, which can yield performance improvements up to 15%. These results emphasize the importance of using state estimation jointly with feedback controllers for efficient operation under situations of measurement noise.

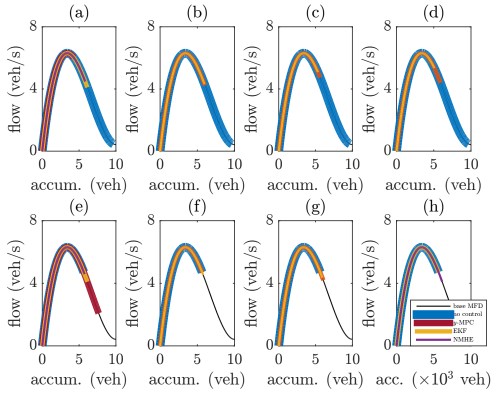

Fig. 6. Outflow MFDs for the congested scenario comparing the no control case, y-MPC, and all measurement configurations with the combined EKF-MPC and MHE-MPC schemes: (a) Region 1 with h_1, (b) region 1 with h_2, (c) region 1 with h_3, (d) region 1 with h_4, (e) region 2 with h_1, (f) region 2 with h_2, (g) region 2 with h_3, (h) region 2 with h_4.

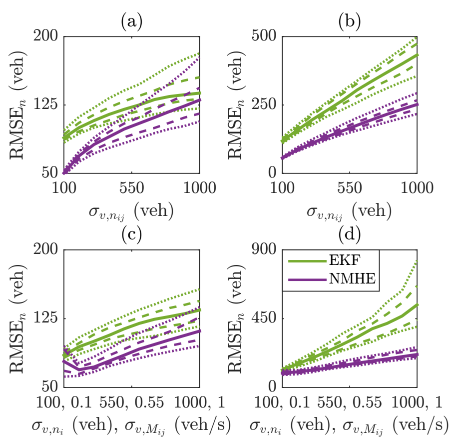

Fig. 7. Sensitivity of accumulation state $n_{ij}(t)$ estimation performance to changes in measurement noise intensity, showing the 10th and 90th (dotted), 25th and 75th (dashed), and 50th (solid) percentiles of RMSE$_n$, for a set of 50 randomly generated scenarios and the four measurement compositions: (a) h_1, (b) h_2, (c) h_3, (d) h_4.

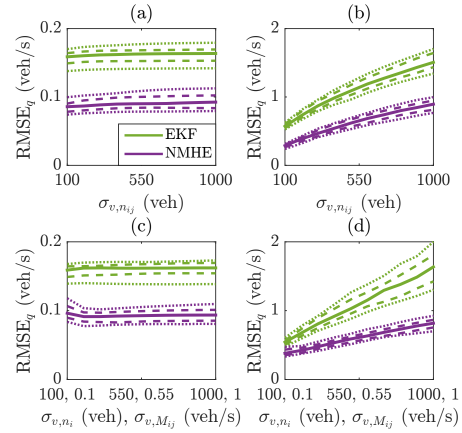

Fig. 8. Sensitivity of inflow demand $q_{ij}(t)$ estimation performance to changes in measurement noise intensity, showing the 10th and 90th (dotted), 25th and 75th (dashed), and 50th (solid) percentiles of RMSE$_q$, for a set of 50 randomly generated scenarios and the four measurement compositions: (a) h_1, (b) h_2, (c) h_3, (d) h_4.

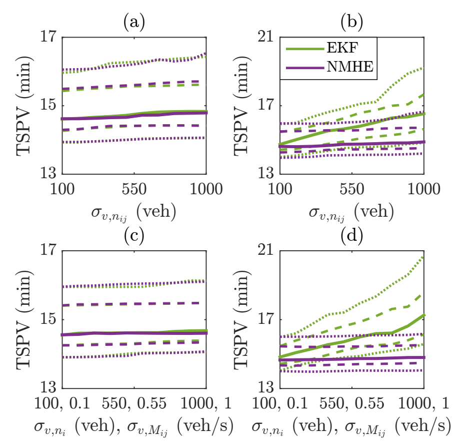

Fig. 9. Sensitivity of control performance to changes in measurement noise intensity, showing the 10th and 90th (dotted), 25th and 75th (dashed), and 50th (solid) percentiles of TSPV, for a set of 50 randomly generated scenarios and the four measurement compositions: (a) h_1, (b) h_2, (c) h_3, (d) h_4.

D. Horizon Length Tuning for MHE

Similar to the case with MPC where its prediction horizon N_c influences control performance (see [36] and [43] for MPC tuning results for a two-region and seven-region urban network, respectively), MHE performance is strongly influenced by the estimation horizon N_e. To study how changing N_e affects estimation and control performance for the combined MHE-MPC scheme, a series of simulation experiments (with a set of 50 randomly generated scenarios) is conducted with varying values of N_e from 1 to 60 (with prediction horizon N_c fixed to 20).

The results are shown in fig. 11, showing RMSE$_n$, RMSE$_q$, and TSPV, as functions of N_e. As expected, estimation performance increases with increasing N_e, especially in the interval $1 \leq N_e \leq 20$, while for $N_e > 20$ the performance increase is not pronounced. It is interesting to note that for measurement compositions h_2 and h_4, RMSE$_q$ decreases with increasing N_e for the whole interval of $1 \leq N_e \leq 30$. This is associated with the fact that these compositions involve measurements on $q_i(t)$ instead of $q_{ij}(t)$, and thus, compared to h_1 and h_3, require more information (i.e., longer horizons) to be able to reconstruct $q_{ij}(t)$. Furthermore, control performance seems to be roughly insensitive to estimation horizon, showing only minor improvement for increasing N_e, suggesting that the MPC is capable of managing congestion when coupled with an MHE, even when said MHE has a short horizon and thus limited estimation performance. Nevertheless, lack of state estimation is catastrophic for the MPC performance when measurement errors are large.

E. Analysis of Constant Future Inflow Demands Assumption

Model predictive perimeter control schemes require inflow demand trajectories for the duration of the prediction horizon into the future (i.e., from time step t to time step $t + N_c - 1$). However, it is exceedingly difficult to know future demands accurately in practice. In order to obtain a practicable MPC scheme, in the formulation given in eq. 21 it is assumed that

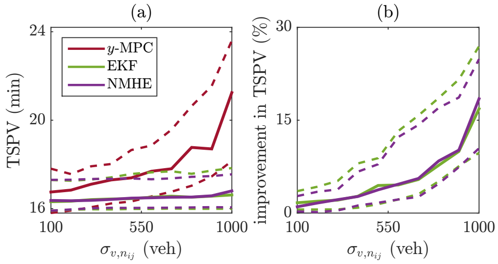

Fig. 10. Sensitivity of control performance to changes in measurement noise intensity, showing the 25th and 75th (dashed), and 50th (solid) percentiles of TSPV and improvement in TSPV, for a set of 50 randomly generated scenarios with high demand: (a) TSPV, (b) improvement in TSPV.

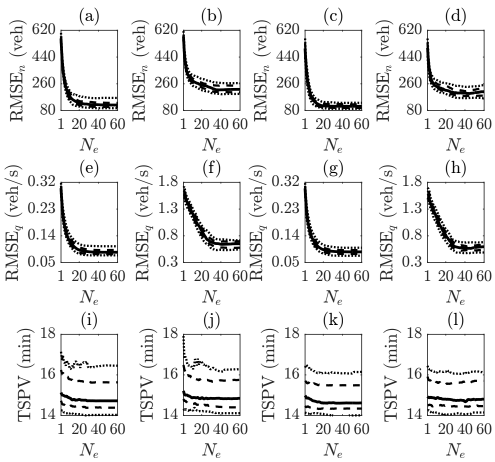

Fig. 11. Estimation and control performance of the combined MHE-MPC scheme as functions of estimation horizon N_e, showing the 10th and 90th (dotted), 25th and 75th (dashed), and 50th (solid) percentiles of (a)-(d) RMSE$_n$, (e)-(h) RMSE$_q$, and (i)-(l) TSPV, for a set of 50 randomly generated scenarios and the four measurement compositions: (a), (e), (i) h_1; (b), (f), (j) h_2; (c), (g), (k) h_3; (d), (h), (l) h_4.

the inflow demands are constant and fixed to their estimated values, which is only a rough approximation since demands vary with time. To examine how assuming constant future demands in the MPC formulation affects control performance of the combined MHE-MPC scheme, a set of 50 randomly generated scenarios is evaluated under the same conditions with the congested scenario, varying only the standard deviations of measurement noise associated with the inflow demands: $\sigma_{v,q_{ij}}$ from 0.1 veh/s to 1 veh/s for the h_1 and h_3 cases; σ_{v,q_i} from 0.1 veh/s to 1 veh/s for the h_2 and h_4 cases. Three different cases are compared (all with the combined MHE-MPC scheme): (a) Future demands are assumed constant and fixed to 0, (b) future demands are assumed constant and fixed to the values estimated by the MHE at time t, (c) future demands are fixed to their true values (i.e., perfect knowledge of demands).

The results are shown in fig. 12, depicting RMSE$_q$, RMSE$_{fq}$, and TSPV as functions of standard deviations associated with inflow demand measurement noise, where RMSE$_{fq}$ is the root-mean-square error expressing the difference between the true inflow demands and the constant trajectories used by the MPC that are fixed to the estimated values at time t, defined for a single simulation experiment as

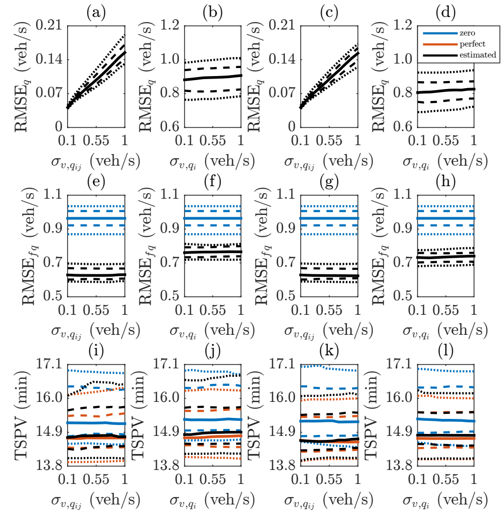

Fig. 12. Inflow demand estimation performance, accuracy of constant future inflow demands assumption, and control performance of the combined MHE-MPC scheme as functions of measurement noise intensity, showing the 10th and 90th (dotted), 25th and 75th (dashed), and 50th (solid) percentiles of (a)-(d) RMSE$_q$, and (e)-(h) RMSE$_{fq}$, and TSPV (i)-(l), for a set of 50 randomly generated scenarios and the four measurement compositions: (a), (e), (i) h_1; (b), (f), (j) h_2; (c), (g), (k) h_3; (d), (h), (l) h_4.

follows:

$$\text{RMSE}_{fq} = \frac{1}{4}\sum_{i=1}^{2}\sum_{j=1}^{2}\sqrt{\frac{\sum_{t=1}^{t_{\text{final}}}\sum_{k=0}^{N_c-1}(q_{ij}(t+k)-\hat{q}_{ij}(t))^2}{t_{\text{final}}\cdot N_c}}. \tag{25}$$

From the figures it can be observed that the combined MHE-MPC scheme is fairly insensitive to changing noise intensity associated with inflow demand measurements, since both RMSE$_{fq}$ and TSPV metrics show limited degradation against increasing noise intensity. Furthermore, the figures comparing TSPV of the three cases show that although assuming constant future inflow demands in the MPC is a rough approximation, it yields control performances that are virtually identical to those obtained by having perfect information on inflow demands. These results suggest that a combined MHE-MPC scheme with an MPC formulation having constant future inflow demands fixed to their estimated values represents a practicable traffic control system that is capable of congestion management without having information on future inflow demands.

V. Conclusion

In this paper we proposed a nonlinear MHE scheme capable of OD inflow demand and accumulation state estimation for a two-region large-scale urban network model with MFD-based dynamics, together with four practically motivated measurement compositions. Observability tests revealed that observability is retained for compositions with limited or no measurements on OD-based information. This has practical significance, since OD-based measurements are usually not available or difficult to obtain in real-time. Extensive simulations show that the estimation performance of the proposed MHE scheme is fairly insensitive to increasing noise intensity, and is superior to an EKF. An important result is that the control performance of the combined MHE-MPC scheme is virtually insensitive to increasing intensity in measurement noise, which is a practically relevant finding considering that perimeter control schemes have to operate under noisy conditions in the field. Further simulations revealed that assuming constant future demands in the MPC formulation yields control performances practically identical to the case with perfect demand information. Overall, the results indicate a strong potential towards implementation of MFD-based perimeter control, since the proposed MHE-MPC scheme is capable of high performance congestion management under severe conditions of measurement noise, limited or no OD-based information, and unknown future inflow demands.

Strong demand fluctuations inducing fast evolving transient states, route choice effects, and spatially heterogeneous distribution of congestion can influence the trip length distribution in the network. These can result, for rapidly evolving traffic conditions, in accumulation-based models relying on the outflow MFD (as approximated by production over trip length) to exhibit inaccuracies due to the MFD ignoring traffic history of the network (i.e., it is memoryless). For example, in case of an inflow demand discontinuity in uncongested conditions, outflow and accumulation predicted by the outflow MFD-based model increase instantaneously, although they should increase only after a delay related to the duration of the shortest trip. Trip-based MFD models (see [56]) and their extensions (see [57]) involving average distance remaining to be traveled as a state specify strong candidates for addressing such concerns associated with accumulation-based model relying exclusively on outflow MFD with production over trip length approximation. Development of control-oriented trip-based models of MFDs networks, and testing their performance in model-based prediction, estimation, and control with detailed microscopic simulations and real-world experiments against accumulation-based models is an important research priority.

Acknowledgment

This research has been supported by the ERC (European Research Council) Starting Grant "METAFERW: Modelling and controlling traffic congestion and propagation in large-scale urban multimodal networks" (Grant # 338205).

References

[1] C. Diakaki, M. Papageorgiou, and K. Aboudolas, "A multivariable regulator approach to traffic-responsive network-wide signal control," *Control Engineering Practice*, vol. 10, no. 2, pp. 183–195, 2002.

[2] K. Aboudolas, M. Papageorgiou, A. Kouvelas, and E. Kosmatopoulos, "A rolling-horizon quadratic-programming approach to the signal control problem in large-scale congested urban road networks," *Transportation Research Part C: Emerging Technologies*, vol. 18, no. 5, pp. 680–694, 2010.

[3] A. Kouvelas, K. Aboudolas, M. Papageorgiou, and E. B. Kosmatopoulos, "A hybrid strategy for real-time traffic signal control of urban road networks," *IEEE Transactions on Intelligent Transportation Systems*, vol. 12, no. 3, pp. 884–894, 2011.

[4] P. Varaiya, "Max pressure control of a network of signalized intersections," *Transportation Research Part C: Emerging Technologies*, vol. 36, pp. 177–195, 2013.

[5] A. Kouvelas, J. Lioris, S. Fayazi, and P. Varaiya, "Maximum pressure controller for stabilizing queues in signalized arterial networks," *Transportation Research Record: Journal of the Transportation Research Board*, no. 2421, pp. 133–141, 2014.

[6] T. Wongpiromsarn, T. Uthaicharoenpong, Y. Wang, E. Frazzoli, and D. Wang, "Distributed traffic signal control for maximum network throughput," in *15th International IEEE Conference on Intelligent Transportation Systems*. IEEE, 2012, pp. 588–595.

[7] A. A. Zaidi, B. Kulcsar, and H. Wymeersch, "Traffic-adaptive signal control and vehicle routing using a decentralized back-pressure method," in *European Control Conference*. IEEE, 2015, pp. 3029–3034.

[8] X. Sun, L. Muñoz, and R. Horowitz, "Highway traffic state estimation using improved mixture kalman filters for effective ramp metering control," in *Decision and Control, 2003. Proceedings. 42nd IEEE Conference on*, vol. 6. IEEE, 2003, pp. 6333–6338.

[9] Y. Wang and M. Papageorgiou, "Real-time freeway traffic state estimation based on extended kalman filter: a general approach," *Transportation Research Part B: Methodological*, vol. 39, no. 2, pp. 141–167, 2005.

[10] A. Messner and M. Papageorgiou, "Metanet: A macroscopic simulation program for motorway networks," *Traffic Engineering & Control*, vol. 31, no. 8-9, pp. 466–470, 1990.

[11] L. Mihaylova, R. Boel, and A. Hegyi, "Freeway traffic estimation within particle filtering framework," *Automatica*, vol. 43, no. 2, pp. 290–300, 2007.

[12] Y. Yuan, J. Van Lint, R. E. Wilson, F. van Wageningen-Kessels, and S. P. Hoogendoorn, "Real-time lagrangian traffic state estimator for freeways," *IEEE Transactions on Intelligent Transportation Systems*, vol. 13, no. 1, pp. 59–70, 2012.

[13] R. Pueboobpaphan and T. Nakatsuji, "Real-time traffic state estimation on urban road network: the application of unscented kalman filter," in *Applications of Advanced Technology in Transportation*, 2006, pp. 542–547.

[14] Q.-J. Kong, Z. Li, Y. Chen, and Y. Liu, "An approach to urban traffic state estimation by fusing multisource information," *IEEE Transactions on Intelligent Transportation Systems*, vol. 10, no. 3, pp. 499–511, 2009.

[15] A. Nantes, D. Ngoduy, A. Bhaskar, M. Miska, and E. Chung, "Real-time traffic state estimation in urban corridors from heterogeneous data," *Transportation Research Part C: Emerging Technologies*, vol. 66, pp. 99–118, 2016.

[16] M. Saeedmanesh and N. Geroliminis, "Clustering of heterogeneous networks with directional flows based on snake similarities," *Transportation Research Part B: Methodological*, vol. 91, pp. 250–269, 2016.

[17] K. An, Y.-C. Chiu, X. Hu, and X. Chen, "A network partitioning algorithmic approach for macroscopic fundamental diagram-based hierarchical traffic network management," *IEEE Transactions on Intelligent Transportation Systems*, vol. 19, no. 4, pp. 1130–1139, 2018.

[18] J. Godfrey, "The mechanism of a road network," *Traffic Engineering and Control*, vol. 11, no. 7, pp. 323–327, 1969.

[19] N. Geroliminis and C. F. Daganzo, "Existence of urban-scale macroscopic fundamental diagrams: Some experimental findings," *Transportation Research Part B: Methodological*, vol. 42, no. 9, pp. 759–770, 2008.

[20] A. Loder, L. Ambühl, M. Menendez, and K. W. Axhausen, "Traffic problems in towns: An empirical analysis with macroscopic fundamental diagrams from cities around the world," in *2018 TRB Annual Meeting: Compendium of Papers*. The National Academies of Sciences, Engineering, and Medicine, 2018, pp. 18–01 049.

[21] J. Haddad and N. Geroliminis, "On the stability of traffic perimeter control in two-region urban cities," *Transportation Research Part B: Methodological*, vol. 46, no. 9, pp. 1159–1176, 2012.

[22] K. Ampountolas, N. Zheng, and N. Geroliminis, "Macroscopic modelling and robust control of bi-modal multi-region urban road networks," *Transportation Research Part B: Methodological*, vol. 104, pp. 616–637, 2017.

[23] R. Zhong, C. Chen, Y. Huang, A. Sumalee, W. Lam, and D. Xu, "Robust perimeter control for two urban regions with macroscopic fundamental diagrams: a control-lyapunov function approach," *Transportation Research Part B: Methodological*, 2017.

[24] M. Keyvan-Ekbatani, M. Papageorgiou, and V. L. Knoop, "Controller design for gating traffic control in presence of time-delay in urban road networks," *Transportation Research Procedia*, vol. 7, pp. 651–668, 2015.

[25] H. Ding, Y. Zhang, X. Zheng, H. Yuan, and W. Zhang, "Hybrid perimeter control for two-region urban cities with different states," *IEEE Transactions on Control Systems Technology*, 2017.

[26] S. Kim, S. Tak, and H. Yeo, "Agent-based network transmission model using the properties of macroscopic fundamental diagram," *Transportation Research Part C: Emerging Technologies*, vol. 93, pp. 79–101, 2018.

[27] H. Fu, N. Liu, and G. Hu, "Hierarchical perimeter control with guaranteed stability for dynamically coupled heterogeneous urban traffic," *Transportation Research Part C: Emerging Technologies*, vol. 83, pp. 18–38, 2017.

[28] H. Ding, F. Guo, X. Zheng, and W. Zhang, "Traffic guidance–perimeter control coupled method for the congestion in a macro network," *Transportation Research Part C: Emerging Technologies*, vol. 81, pp. 300–316, 2017.
[29] C. Menelaou, P. Kolios, S. Timotheou, C. Panayiotou, and M. Polycarpou, "Controlling road congestion via a low-complexity route reservation approach," *Transportation research part C: emerging technologies*, vol. 81, pp. 118–136, 2017.
[30] S. Kim, S. Tak, and H. Yeo, "Investigating transfer flow between urban networks based on a macroscopic fundamental diagram," *Transportation Research Record*, vol. 2672, no. 20, pp. 75–85, 2018.
[31] J. Haddad, "Optimal perimeter control synthesis for two urban regions with aggregate boundary queue dynamics," *Transportation Research Part B: Methodological*, vol. 96, pp. 1–25, 2017.
[32] ——, "Optimal coupled and decoupled perimeter control in one-region cities," *Control Engineering Practice*, vol. 61, pp. 134–148, 2017.
[33] A. Aalipour, H. Kebriaei, and M. Ramezani, "Analytical optimal solution of perimeter traffic flow control based on mfd dynamics: A pontryagin's maximum principle approach," *IEEE Transactions on Intelligent Transportation Systems*, 2018.
[34] A. Kouvelas, M. Saeedmanesh, and N. Geroliminis, "Enhancing model-based feedback perimeter control with data-driven online adaptive optimization," *Transportation Research Part B: Methodological*, vol. 96, pp. 26–45, 2017.
[35] J. Haddad and Z. Zheng, "Adaptive perimeter control for multi-region accumulation-based models with state delays," *Transportation Research Part B: Methodological*, 2018. [Online]. Available: https://doi.org/10.1016/j.trb.2018.05.019
[36] N. Geroliminis, J. Haddad, and M. Ramezani, "Optimal perimeter control for two urban regions with macroscopic fundamental diagrams: A model predictive approach," *IEEE Transactions on Intelligent Transportation Systems*, vol. 14, no. 1, pp. 348–359, 2013.
[37] M. Hajiahmadi, J. Haddad, B. De Schutter, and N. Geroliminis, "Optimal hybrid perimeter and switching plans control for urban traffic networks," *IEEE Transactions on Control Systems Technology*, vol. 23, no. 2, pp. 464–478, 2015.
[38] M. Ramezani, J. Haddad, and N. Geroliminis, "Dynamics of heterogeneity in urban networks: aggregated traffic modeling and hierarchical control," *Transportation Research Part B: Methodological*, vol. 74, pp. 1–19, 2015.
[39] A. Csikós, T. Charalambous, H. Farhadi, B. Kulcsár, and H. Wymeersch, "Network traffic flow optimization under performance constraints," *Transportation Research Part C: Emerging Technologies*, vol. 83, pp. 120–133, 2017.
[40] K. Yang, N. Zheng, and M. Menendez, "Multi-scale perimeter control approach in a connected-vehicle environment," *Transportation research procedia*, vol. 23, pp. 101–120, 2017.
[41] Z. Zhou, B. De Schutter, S. Lin, and Y. Xi, "Two-level hierarchical model-based predictive control for large-scale urban traffic networks," *IEEE Transactions on Control Systems Technology*, vol. 25, no. 2, pp. 496–508, 2017.
[42] M. Ramezani and M. Nourinejad, "Dynamic modeling and control of taxi services in large-scale urban networks: A macroscopic approach," *Transportation Research Part C: Emerging Technologies*, vol. 94, pp. 203–219, 2018.
[43] I. I. Sirmatel and N. Geroliminis, "Economic model predictive control of large-scale urban road networks via perimeter control and regional route guidance," *IEEE Transactions on Intelligent Transportation Systems*, vol. 19, no. 4, pp. 1112–1121, April 2018.
[44] M. Yildirimoglu, I. I. Sirmatel, and N. Geroliminis, "Hierarchical control of heterogeneous large-scale urban road networks via path assignment and regional route guidance," *Transportation Research Part B: Methodological*, vol. 118, pp. 106–123, 2018.
[45] M. Yildirimoglu, M. Ramezani, and N. Geroliminis, "Equilibrium analysis and route guidance in large-scale networks with MFD dynamics," *Transportation Research Part C: Emerging Technologies*, vol. 59, pp. 404–420, 2015.
[46] I. I. Sirmatel and N. Geroliminis, "Moving horizon demand and state estimation for model predictive perimeter control of large-scale urban networks," in *2019 18th European Control Conference (ECC)*. IEEE, 2019, pp. 3650–3655.
[47] R. Hermann and A. Krener, "Nonlinear controllability and observability," *IEEE Transactions on Automatic Control*, vol. 22, no. 5, pp. 728–740, 1977.
[48] H. G. Kwatny and G. Blankenship, *Nonlinear Control and Analytical Mechanics: A Computational Approach*, ser. Control Engineering. Birkhäuser Basel, 2000.
[49] M. N. Chatzis, E. N. Chatzi, and A. W. Smyth, "On the observability and identifiability of nonlinear structural and mechanical systems," *Structural Control and Health Monitoring*, vol. 22, no. 3, pp. 574–593, 2015.
[50] M. Diehl, H. J. Ferreau, and N. Haverbeke, "Efficient numerical methods for nonlinear mpc and moving horizon estimation," in *Nonlinear model predictive control*. Springer, 2009, pp. 391–417.
[51] H. G. Bock and K.-J. Plitt, "A multiple shooting algorithm for direct solution of optimal control problems," in *Proceedings of the IFAC World Congress*, 1984.
[52] M. J. Risbeck and J. B. Rawlings, "MPCTools: Nonlinear model predictive control tools for CasADi (Octave interface)," 2016. [Online]. Available: https://bitbucket.org/rawlings-group/octave-mpctools
[53] J. A. Andersson, J. Gillis, G. Horn, J. B. Rawlings, and M. Diehl, "CasADi: A software framework for nonlinear optimization and optimal control," *Mathematical Programming Computation*, pp. 1–36, 2018.
[54] A. Wächter and L. T. Biegler, "On the implementation of an interior-point filter line-search algorithm for large-scale nonlinear programming," *Mathematical Programming*, vol. 106, no. 1, pp. 25–57, 2006.
[55] E. L. Haseltine and J. B. Rawlings, "Critical evaluation of extended Kalman filtering and moving-horizon estimation," *Industrial & engineering chemistry research*, vol. 44, no. 8, pp. 2451–2460, 2005.
[56] R. Lamotte and N. Geroliminis, "The morning commute in urban areas with heterogeneous trip lengths," *Transportation Research Part B: Methodological*, vol. 117, pp. 794 – 810, 2018, tRB:ISTTT-22. [Online]. Available: http://www.sciencedirect.com/science/article/pii/S0191261517307208
[57] R. Lamotte, M. Murashkin, A. Kouvelas, and N. Geroliminis, "Dynamic modeling of trip completion rate in urban areas with mfd representations," in *Transportation Research Board 97th Annual Meeting*, no. 18-06192, 2018.

Isik Ilber Sirmatel received the B.Sc. degrees in mechanical and control engineering from Istanbul Technical University, Turkey, and the M.Sc. degree in mechanical engineering from Swiss Federal Institute of Technology in Zurich, Switzerland, in 2010, 2012, and 2014, respectively. He is currently working toward the Ph.D. degree in electrical engineering at the Urban Transport Systems Laboratory (LUTS), School of Architecture, Civil and Environmental Engineering, Swiss Federal Institute of Technology in Lausanne (EPFL), Switzerland. His research interests include automatic control, optimization, and model predictive control, with applications to control of transportation systems.

Nikolas Geroliminis is an Associate Professor at EPFL and the head of the Urban Transport Systems Laboratory (LUTS). Before joining EPFL he was an Assistant Professor on the faculty of the Department of Civil Engineering at the University of Minnesota. He has a diploma in Civil Engineering from the National Technical University of Athens (NTUA) and an M.Sc. and Ph.D. in civil engineering from University of California, Berkeley. He is a member of the Transportation Research Board's Traffic Flow Theory Committee. He also serves as an Associate Editor in Transportation Research, part C, Transportation Science and IEEE Transactions on ITS and in the editorial board of Transportation Research, part B, Journal of ITS and of many international conferences. His research interests focus primarily on urban transportation systems, traffic flow theory and control, public transportation and logistics, on-demand transportation, optimization and large scale networks. He is a recent recipient of the ERC starting grant "METAFERW: Modeling and controlling traffic congestion and propagation in large-scale urban multimodal networks".